Nanoscale

Accepted Manuscript

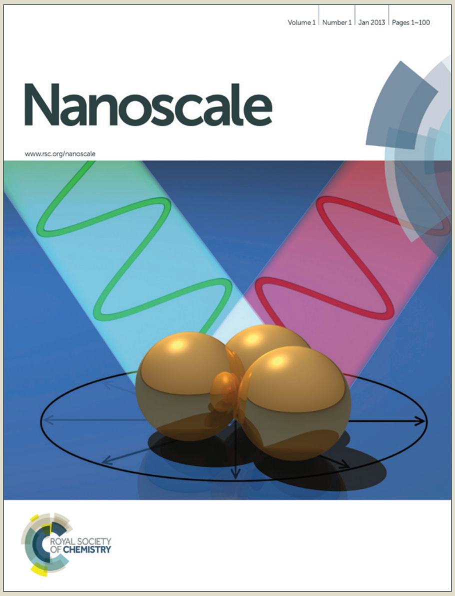

ROYAL SOCIETY OF CHEMISTRY

www.rsc.org/nanoscale

Nanoscale

ARTICLE

Received 00th January 20xx,

Accepted 00th January 20xx

DOI: 10.1039/x0xx00000x

www.rsc.org/

Oxygen vacancies and intense luminescence in manganese assisted ZnO microflowers for visible light water splitting

Balaji Sambandam[a], Robin Jude Vimal Michael[a], and Periakaruppan T Manoharan[*a]

ZnO nanorods and Mn/ZnO microflowers with nano-sized petals exhibit singly ionized oxygen vacancy, V^{+}_{O} which is strongly supported by photoluminescent green emission at 2.22 eV and EPR g value of 1.953 which are suppressed greatly after annealing in oxygen atmosphere. A strong red emission observed during its exposure to X-ray reveal the presence of F^{+} centres as a consequence of V^{+}_{O}. Mn/ZnO displayed enhanced H_2 generation to visible light exposure, when compared to pure ZnO and annealed Mn/ZnO in the visible region as they directly well corroborate with oxygen vacancies concentration. There is an interesting correlation between the intensities of EPR lines at the g-value of 1.953 due to oxygen vacancy, intensity of light emitted by exposure to X-ray, the intensity of photoluminescence due to oxygen vacancy and the quantity of H_2 production by photocatalytic effect on comparing the three different nanomaterials, *viz.* pure ZnO, Mn/ZnO before and after annealing, all having been made exactly by the same methodologies.

Introduction

Controversy exists on the assignment of various emissions in photoluminescence (PL) experiments of ZnO such as from shallow donors, singly ionized oxygen (V^{+}_{O}), Zn vacancies (V_{Zn}), oxygen and zinc interstitials (O_i and Zn_i). There is a similar controversy on the g-values of ~1.96 and ~1.99 from electron paramagnetic resonance (EPR).[1] The EPR signal at g ~ 1.99 especially for conduction band electrons is also close to the free electron g = 2.0023 and hence it can be omitted from this competition. However, a real competition among the species of V^{+}_{O}, V_{Zn}, and O_i is for conquering g = ~ 1.96.[2]

V^{+}_{O} (vacancy of oxygen occupied by an electron, hence paramagnetic) is a quite common vacancy observed in zinc oxide materials. Particularly it is well known that this nanomaterial of ZnO characteristically exhibits this vacancy despite the method of making it with or without additional component such as a metal ion specially a divalent one. Hence it is expected that the additional component may have its effect on its morphology modification and other physical properties such as photoluminescence, magnetism and many more along with changing is application potential. One of the most recent work deals with such oxygen vacancies in pure zinc oxide[3] while our work deals with the effect of additional metal ion incorporation in this lattice. This defect centre may also be attributed to F^{+} centers, normally observed in alkali halide.[4]

Previous studies clearly indicate that many tunable parameters such as particle size[5], concentration of oxygen defects,[6,] surface area[7] and exposed facets[8] are required to improve the photocatalytic activity of ZnO. Among them, oxygen defects are proposed to be the active sites of the ZnO photocatalyst, however, high concentration of the defects suppresses the activity. It is noteworthy to mention that the optimum concentration of oxygen defects for photocatalytic activity can be determined by various photo-physical characterisation techniques such as EPR, PL and thermal analysis.

ZnO can be prepared by a variety of methods depending on its use for specific purpose as seen in review paper of Radzimska *et al.*[9] Magnetic doping such as with Cu, Mn, Fe, etc., can not only change the host's physical properties like lattice contraction/elongation, morphology, size, etc., but also can tune the photo-physical, magnetic and other resultant properties. Though highly interesting, our current emphasis is not about magnetism but mostly pertains to EPR g values and the photo-physical properties of such materials with manganese and its consequence to photocatalysis. The microstructural properties of ZnO is also very relevant in deciding the above-said properties and ZnO can be present as nanorods, nanowires, nanobelts, nanocrystals and nanosheets. There is, however, a beautiful transformation of ZnO nanorods to microflowers during the current observation of Mn inclusion. Such kind of transformations during such addition of metal ions have been rarely observed such as during the addition of Ag and Au in our own earlier work.[10,11] The most interesting aspect comes from our current observation of H_2 generation from Mn containing ZnO materials, a new one, probably the first such report using Mn, we believe.

---

[a] *Department of Chemistry. Indian Institute of Technology-Madras, Chennai-60036*
E-mail: ptm@iitm.ac.in

Electronic Supplementary Information (ESI) available: [details of any supplementary information available should be included here]. See DOI: 10.1039/x0xx00000x

Furthermore there seems to be a relation between the presence of oxygen vacancies and introduction of Mn.

Modified ZnO and ZnO based heterostructures display visible light photocatalytic water splitting hydrogen production in recent years. Lu *et al.*[12] shows surface hydrogenated ZnO nanorods achieves a high productivity of 122500 µmol h^{-1} g^{-1} of hydrogen opened a new possibility of tuning this material for higher efficiency. They explained this higher activity due to presence of surface oxygen vacancies (V_O) as well as interstitial hydrogen (H_i) and former acting as a hole trap that enhances the separation of the electron–hole pairs. Recently, In_2O_3/ZnO heterostructure exhibits 176 µmol h^{-1} (0.1 g) of hydrogen in presence of aqueous methanol.[13] Another interesting and high yield hydrogen production observed from yttrium and aluminium co-doped ZnO nanoparticles. This nanoparticle produces 5710 µmol h^{-1} g^{-1} of hydrogen in presence of aqueous solution containing 15 vol% of lactic acid.[14] Sulfonated graphene and silver based ZnO composite[15] (SG/ZnO/Ag) evolved 2360 µmol h^{-1} g^{-1} of hydrogen under the UV light. Gomathisankar *et al.*[16] harvested nearly 933 and 224 µmol h^{-1} g^{-1} of hydrogen from B/CuO/ZnO heterostructure under xenon lamp irradiation with and without the cut filter (>400 nm), respectively.

Taking into account of the advantages of ZnO with oxygen vacancies, here we demonstrate hydrogen production from manganese doped ZnO micro-flowers using a low power light source of 150 W.

Experimental

Synthesis of strong luminescent ZnO

In typical synthesis of micro-flowers of ZnO, 0.5 M of zinc acetate and 5 M of NaOH dissolved in 60 mL of Millipore water and 10 ml of butylene diamine stirred for 30 minutes and transferred into Teflon lined Stainless Steel autoclave of 300 mL capacity. The final volume of the reactants is adjusted to 80 % by adding Millipore water. The autoclave with reactants is kept in hot air oven preheated to 160 ˚C for 12 hours. After cooling the precipitated zinc oxide are decanted from the solution and washed several times with millipore water and ethanol and kept for drying at 80 ˚C for evaporation of the solvents. The same procedure is repeated except with manganese acetate to synthesize ZnO/Mn(5%).

Photocatalytic Hydrogen evolution

Photocatalytic hydrogen evolution was performed in external irradiation type Pyrex reactor (Volume 60 ml) with 150 W medium high pressure metal halide lamp (OSRAM HCLB22) as the light source. The Spectral power distribution of the lamp output is of the wavelength from 350 nm to 800 nm. Any radiation below 400nm is filtered off using band pass filter. The temperature of the reactor was maintained below 35˚C by cooling water circulation. In a typical run, photocatalyst of 60 mg was dispersed well in 60 mL aqueous solution containing 20% Methanol by constant stirring for two hours in order to allow catalyst adsorption. The reactor was bubbled with argon and evacuated many times to remove any air or oxygen impurities and filled with argon gas finally. The 0.5 µL of the gas was collected intermittently from the reactor headspace through gastight syringe and analyzed by Newcon Gas chromatograph equipped with molecular sieve column, TCD detector, and argon as carrier gas.

Characterizations

Powder XRD measurements were done by Bruker Discover D8 with default background correction. Solid state UV-Vis measurements were performed by using a Cary 5E UV-VIS-NIR spectrophotometer. Photoluminescence measurements were carried out with JOBIN YUON Fluorolog-3-11. X-ray photoelectron spectroscopy (XPS) measurements were done using an Omicron ESCA Probe spectrometer with polychromatic MgKα X-rays (hυ=1253.6 eV). HRSEM measurements were performed using FEI Quanta FEG 200. Electron Paramagnetic Resonance (EPR) analysis were done using Bruker X- band CW EPR.

Results and discussion

Powder XRD profiles for butyldiamine (BD) mediated pure ZnO, 5% manganese assisted ZnO and annealed Mn/ZnO in oxygen atmosphere at 400 ˚C are shown in Fig. 1(a). All are indexed exactly with hexagonal ZnO pattern and (101) plane at 2θ = 36.2˚ magnified in Fig. 1(b) infers the lattice spacing on incorporation of manganese into the ZnO frame. It confirms that addition of manganese as well as annealing results in lattice contraction (Mn/ZnO) and elongation (Mn/ZnO annealed) as revealed by a shift in the 2θ values. These expansion and contraction are due to concentration of oxygen vacancies[17] (F^+ centres and manganese-oxygen interaction) and manganese incorporation in the interstitial position**.** The plane around 18.2˚ found both in Mn/ZnO and annealed Mn/ZnO has a common region for (101) plane of $ZnMn_2O_4$ (18.2˚, JCPDS file:77-0470) and (111) plane of $ZnMnO_3$ (18.3˚, JCPDS file:19-1461) where the oxidation states of manganese are +3 and +4 respectively. The observed planes of (112), (103) and (211) respectively at 29.5˚, 33.2˚ and 36.41˚ confirm the

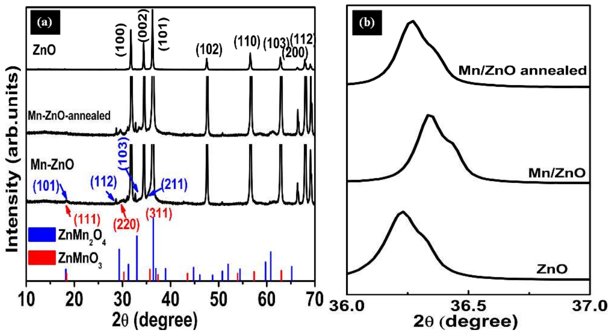

Fig. 1 (a) XRD profiles for pure ZnO, 5%Mn-ZnO and annealed 5%Mn-ZnO in O_2 atmosphere. JCPDS file for $ZnMn_2O_4$ and $ZnMnO_3$ are plotted at the bottom (b) expanded version of (101) plane of ZnO at 36.2˚ for all above three.

formation of $ZnMn_2O_4$ and those of (220) and (400) match respectively at 30.2˚ and 43.5˚ prove the formation of $ZnMnO_3$ in both materials. However, between the two secondary phases, $ZnMnO_3$ planes become intense in the XRD pattern after annealing the material in oxygen atmosphere.

UV-Vis-DRS profile for these materials is shown in the Fig. 2. There is a strong absorption between 400 – 800 nm regions in manganese samples revealing incorporation enhance the visible activity. This could be connected with the appearance of the various impurity levels in the forbidden gap after manganese introduction. Further, few weak absorption cusps or shoulders observed around 410, 520, 620 and 730 nm are due to various crystal field transitions of both Mn^{3+} and Mn^{4+} states (see XPS).[18] There is a small red shift in band gap of Mn/ZnO prior to annealing revealing high band gap narrowing in comparison to annealed Mn/ZnO and Mn free ZnO. The long visible tail of absorption in manganese samples may also be due to absorption edges[19] of $ZnMn_2O_4$, secondary phase in our system.

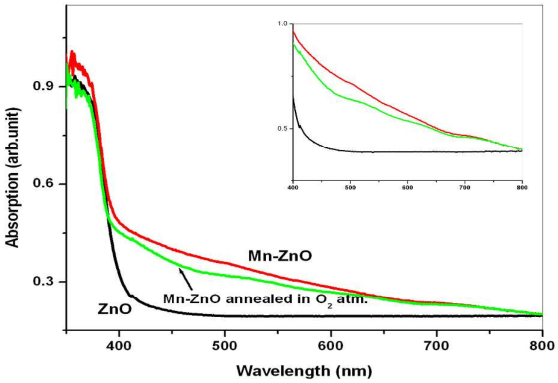

Fig. 2 UV-DRS for ZnO and 5%Mn- ZnO nanostructure (as synthesized and annealed in Oxygen atmosphere at 400˚C)

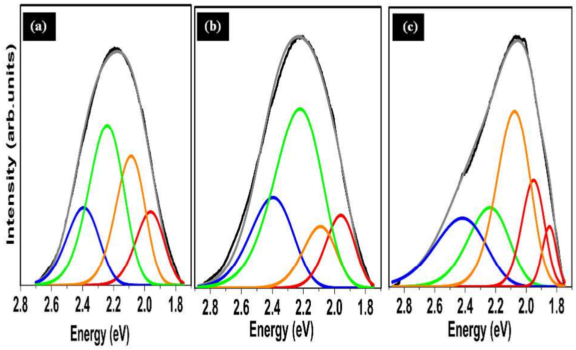

Fig. 3 Deconvoluted Photoluminescence energy profiles for (a) pure ZnO, (b) Mn/ZnO and (c) O_2 atmosphere annealed Mn/ZnO.

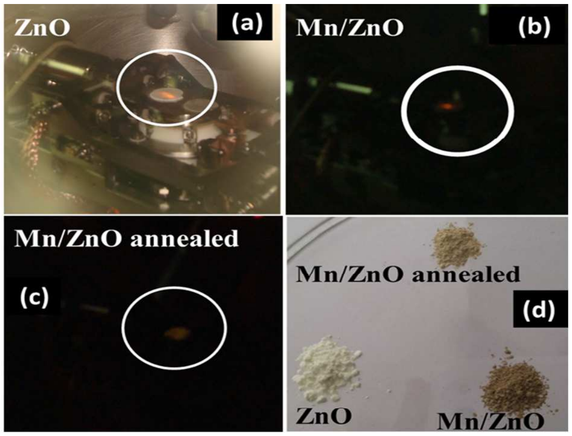

Fig. 4. XPS photographs of ZnO microflowers during analysis. A red emission observed when x-rays hit the samples; (a) ZnO (b) Mn/ZnO (c) annealed Mn/ZnO and (d) photograph images of powder materials.

Fig. 3 shows the deconvoluted energy profile from the PL of ZnO, Mn/ZnO and annealed samples when excited at 300 nm. The overall wavelength emission profile of ZnO of this work before deconvolution looks similar to that of ZnO_{1-x} of the work of *Guo et al.*[3] The near band emission (NBE) for all three material as given ESI Fig. S1 reveal a red shift emission among these materials and forbidden gap emission (defects emission) predominant over the band gap emission. It is significant to deconvoulte the as-symetric forbidden gap emissions to sort out various energy levels. In the current work on deconvoluted energy profile, the emission at 2.40 eV is due to oxygen antisite[20] i.e., zinc ions are placed in oxygen lattice (O_{Zn}) found in all three materials. The major emission at 2.22 eV falls in the region of green and is said to be due to oxygen defects centers,[21] i.e., $V^{+}o$ as well as to zinc vacancy,[22] V_{Zn} raising a controversy. The intensity of oxygen defects emission in our experiments is enhanced on introducing manganese into the ZnO microflowers but gets decreased considerably in Mn/ZnO microflowers obtained after annealing in O_2 atmosphere due to the incoming oxygen partially occupying the oxygen vacancy sites. This emission could also be due to F^+ centers[4] i.e., $V+_O$ in our above description. This assignment can be confirmed by the observation of a strong fluorescent light emitted during its exposure to X-radiations as shown in Fig. 4. It is direct evidence of F^+ centres as a consequence of oxygen vacancies. As seen in Fig.4 the emission intensity increases in the order: annealed Mn/ZnO < ZnO < Mn/ZnO prior to annealing. Thus F^+ intensity is reduced greatly in Mn/ZnO annealed sample due to the occupation of oxygen vacancies by incoming oxygen. Hence the emission at 2.22 eV is attributed to V^{+}_{O}. Yet another emission at 2.07 eV is owing to oxygen in the interstitial position, O_i.[23] The presence of this emission in pure ZnO gets reduced after manganese incorporation (Mn/ZnO microflowers) and is again getting enhanced on annealing in presence of O_2. This enhancement can be explained by partial reoccupation of those interstitial sites by oxygen (oxygen atmosphere) in annealed Mn/ZnO microflowers. The emission at 1.96 eV, originates from $V_{Zn.}$ This red emission centered at 630 nm originates from the electron transition[24] of $V^{+}_{O} \rightarrow V^{-}_{Zn}$ which is present in all three materials. There is no appropriate change in the intensity of emission in pure and Mn/ZnO materials, however, its intensity decreased on annealing since annealing can partially reduce the defects. It is noteworthy to mention that another emission observed at 1.79 eV present only in annealed Mn/ZnO is caused by electron transition $V^{+}_{O} \rightarrow O_{i}$.[25] The graphical representation of all transitions are given in ESI Scheme I.

The high resolution scanning electron microscopy (HRSEM) images of as synthesized ZnO and Mn/ZnO nanomaterials are shown in Fig. 5a and 5b respectively. It is clear that the as-synthesized ZnO nanomaterials show rods-like morphology and tends to transform into a flower like structure on introducing Manganese. The width of the flower petals at the centre are in the range of few hundred nanometers while at the tip it is less than 100 nm. The morphology changes may due to the faster reaction rate originating from the higher manganese concentration. Recently Sotillo *et al.*[26] addressed that dopant ion concentration influence the morphology changes in ZnS nanostructures. They concluded that the strain induced by the size difference between the In ion and the Zn ion of the host leading to difference in its morphology. Similarly, ZnO feels high strain in the form of vacancies after introduction of Mn ions (as proven by PL and EPR) leads to different morphology. However, the mechanism for the transformation requires in depth study by varying Mn ions concentration.

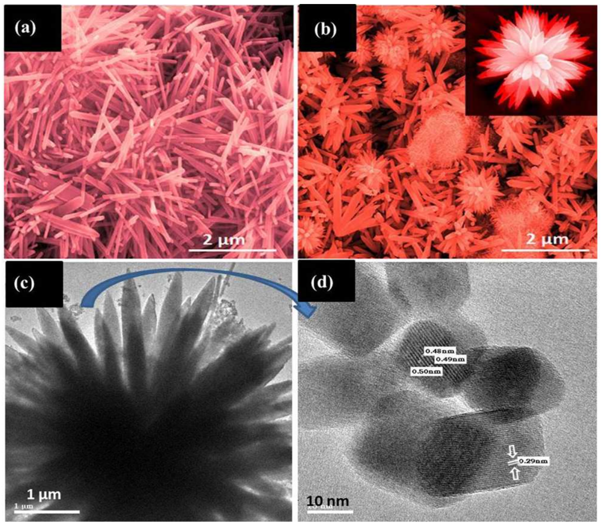

Fig. 5 HRSEM images of (a) ZnO and (b) Mn/ZnO microflowers with nano-sized petals. Inset: single microflowers. (c) HRTEM image of single Mn/ZnO microflower and (d) magnified image of small decorated secondary phases of nanoparticles of $ZnMn_2O_4$ and $ZnMnO_3$ on ZnO microflowers.

Fig. 5c shows HRTEM image of flower like morphology of Mn/ZnO with clear petals. It is interesting to note that the two ternary alloys of $ZnMn_2O_4$ and $ZnMnO_3$ are decorated on the surface of ZnO microflowers as shown in the image. Fig. 5d represents magnified image of small particles nearer the surface of ZnO microflowers. The measured particles size is in the range of 15-30 nm. The HRTEM measurements clearly show the lattice fringes with d = 0.24 nm (in another image but not shown in 5(d)) which match well with that of 0.246 nm corresponding to the (211) crystallographic plane of $ZnMn_2O_4$ as measured by Zhang et al.[19] It is the strongest crystallographic plane, corresponding to the distance between (211) crystal planes of the spinel phase of this zinc manganese oxide as we have also seen in our XRD pattern. Similarly we also noticed the presence of lattice fringes with 0.29 nm spacing which probably is the same as that found in the TEM images of $ZnMnO_3$ nanoflakes at 0.29 nm (220 plane) reported by Jaćimović and coworkers.[27] The other d spacings measured by us at 0.17 nm and 0.48-0.50 nm may be from either the (422) of $ZnMnO_3$/(105) of $ZnMn_2O_4$ and (111) of $ZnMnO_3$/(101) of $ZnMn_2O_4$ nanoparticles, however, we do not have definite proof. More HRTEM images show the decorated particles on the surface of the ZnO flowers as given in ESI Fig.S2. Indeed the decoration of these two phases mostly uniform throughout the flowers as shown in ESI Fig.S2 (a) and (b) at the same time it is difficult to distinguish of two phases from the electron microscopy. Few particles even buried in the flower's petals also been seen in ESI Fig. S2(b). The SAED pattern of Mn/ZnO shows (ESI Fig. 2(e) and 2(f)) no phase purity among these competitors revealing mixed phases throughout the structure.

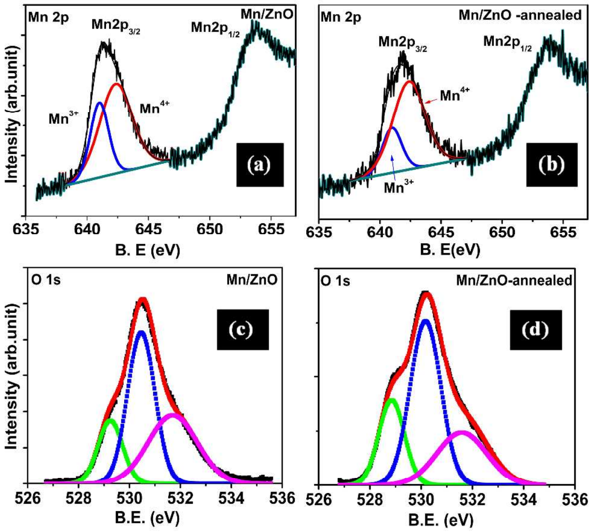

Fig. 6 XPS Mn 2p profile for (a) Mn/ZnO and (b) annealed Mn/ZnO. Similarly O 1s for (c) Mn/ZnO and (d) annealed Mn/ZnO.

The deconvoluted XPS Mn $2p_{3/2}$ lines for Mn/ZnO and annealed sample are shown in Fig. 6a and 6b respectively. The broad $Mn2p_{3/2}$ peaks in both samples reveal the presence of both Mn^{3+} and Mn^{4+} species respectively at 641.5 eV and 642.8 eV. This has been achieved through deconvolution. The line at 641.5eV corresponds to Mn^{3+} oxidation state as evidenced by other methods *viz* powder diffraction and UV-DRS. The other oxidation state of Mn^{4+} shows its $Mn2p_{3/2}$ line at 642.8 eV correlates well with other published reports.[28] The quantification of each oxidation states agrees well with XRD profile as one of the secondary phases, $ZnMnO_3$ (where manganese has +4 oxidation state) predominates over the other, $ZnMn_2O_4$ with +3 oxidation state. The deconvolution also shows that secondary phase, $ZnMnO_3$, comes out even more pronounced after annealing adding to the evidence from XRD. We see the corresponding peak due to $Mn2p_{1/2}$ but we did not make an attempt at further analysis except for noting the binding energy separation between the peaks due to

$Mn2p_{3/2}$ and $Mn2p_{1/2}$ normally being separated by around 12 eV. Survey spectrum for these materials has been given in ESI Fig. S3.

The XPS for O1s in Mn/ZnO sample shows three different oxygen environments in Fig. 6c. The one at lower binding energy is 528.9 eV due to O_i; the second at 530.5 eV for (O^{2-}) from the lattice of the ZnO and higher binding energy at 531.6 eV is due to V^+_O.[29] However, the same line at 528.9 eV after annealing at 400 ˚C in O_2 atmosphere (Fig. 6d) shows enhanced line intensity due to increased number of O_i species in presence of oxygen environment (during annealing). The same kind of process has taken place in lattice O^{2-} as it shows larger line width comparable to as-synthesized Mn-ZnO microflowers (prior to annealing). On the other hand, the O1s peak for oxygen defects (V^+_O) is getting reduced as incoming oxygen partially occupies the defects.

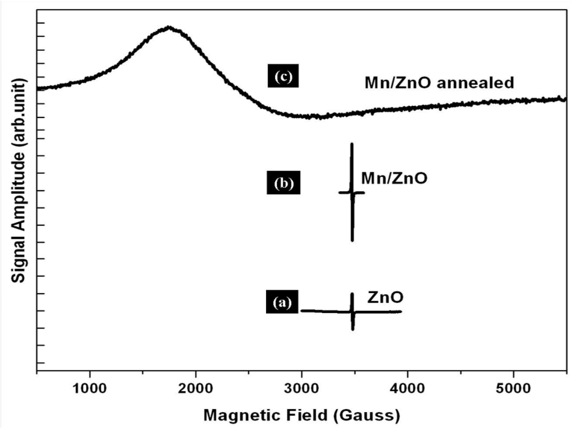

Fig. 7 Room temperature EPR spectra for (a) pure ZnO (b) Mn/ZnO and (c) annealed Mn/ZnO under O_2 atmosphere at 400 °C.

EPR spectroscopy has been used to identify magnetically active defects/vacancies in the crystalline structures. Thus ZnO and Mn/ZnO shows only the sharp EPR signal at g = 1.9532 with measured line width of less than 5 G as seen in Fig. 7a and 7b. There is, however, a controversy over the interpretation of the signal of g ~ 1.95. Some reports[1,2,30] suggest it to be due to conduction band electrons or shallow donors. Some others reports assign this value is due to electrons from the conduction band getting trapped in oxygen vacancy. The latter assignment reveals the presence of strong singly ionized oxygen vacancies (V^+_O).[21,31] This explanation is supported by the results of PL where the oxygen vacancies emission dominates over other emissions and its intensity increase with incorporation of manganese, while annealing in O_2 atmosphere it gets decreased. Hence the agreement between the EPR g value of ~1.96 and the high intensity of PL emission on oxygen vacancies (V^+_O). It is very interesting to see that EPR g-value in the work of Guo *et al.*[3] on ZnO_{1-x} turns out to be 2.01 attributed to be due to O_2^- and not due to oxygen vacancy which has a g value of ~1.96 as in our work. However, it is perplexing to note that there is no evidence for the presence of manganese signal in the EPR profile (Fig. 7b) of Mn/ZnO prior to annealing despite strong evidences for the presence of manganese from other characterizations, *viz.* XPS and XRD. Furthermore, the manganese in ZnO has two different oxidation states, Mn^{3+} and Mn^{4+} arising from the two secondary phases of $ZnMn_2O_4$ and $ZnMnO_3$ respectively. The former has d^4 with S = 2 or 1 (depending on the nature of ligand field; in the present system S=2 is favoured) and latter has d^3 (S = 3/2) configurations. It may be noted that the electronic configurations of both the systems may be described respectively as $(e)^2(t_2)^2$ and $(e)^2(t_2)^1$, both being in a tetrahedral environment of oxygen ligands and both being electronically fast relaxing systems and hence the EPR silent nature of d^4 $ZnMn_2O_4$, and d^3 $ZnMnO_3$ even at liquid nitrogen temperature. The EPR silent property of manganese in d^4, $ZnMn_2O_4$ may also be interpreted as due to fast electron exchange between the two manganese centres either by long distance charge transfer or short distance faster exchange.

However, an interesting EPR behaviour of Mn/ZnO was noticed after annealing at 400 ˚C in presence of oxygen atmosphere, as shown in Fig. 7c. The oxygen defect signal of g =1.95 disappeared since these defect oxygen vacancies were being filled by incoming oxygen.[31] Sometimes it appears as a very low intensity signal due to incomplete occupation. On the other hand, a new broad signal with g value of ~ 3.7 observed needs a new kind of explanation and mechanism. The latter signal has been observed very rarely and that too not with such a great intensity. Such a signal can be observed from Mn^{4+} ion with a d^3 configuration as present in $ZnMnO_3$. Part of this intense signal could also come from a coupling between Mn^{3+}, a d^4 ion present in $ZnMn_2O_4$ and left over V^+_O as revealed by the much reduced intensity of green emission at 2.2ev. The high intensity of the EPR line at g~3.7 must have been due to the above-said two different d^3 configurations, one from the Mn^{4+} of $ZnMnO_3$ and other from the coupling between Mn^{3+} of $ZnMn_2O_4$ and V^+_O. However, the most important point pertains to the presence of $ZnMn_2O_4$ and $ZnMnO_3$ and the part played by them in PL.

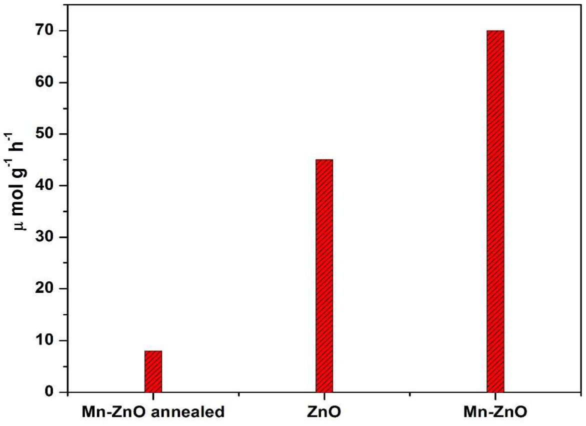

Fig. 8 Photocatalytic visible light water splitting hydrogen generation for ZnO and Mn assisted ZnO.

It is already reported that oxygen defects enhance the photocatalytic activity.[32] This could further be supported by the presence of F^+ centres of V^+_O defects. Hence we looked into the photophysical insights of these materials by carrying out the water splitting experiments. Fig. 8 shows the photocatalytic activity of three different samples, pure ZnO, Mn/ZnO prior to and after annealing.

Photocatalytic water splitting hydrogen generation is performed in a home-made reactor under visible light. The detailed experimental procedure is given in experimental. The measured hydrogen was found to be ~ 70 μ mol g^{-1} h^{-1} for Mn/ZnO prior to annealing when compared to ~ 45 μ mol g^{-1} h^{-1} of pure ZnO and a meagre ~ 8 μ mol g^{-1} h^{-1} for Mn/ZnO after annealing. A suitable interpretation for this observation can be provided on the basis of earlier work and by correlating to our own photoluminescence spectral behaviour.

It has been reported earlier that oxygen vacancy concentration, especially on the surface, has an important role to play in influencing light absorption of the photocatalyst.[33] Furthermore, the photocatalytic activity is said to be is due to band gap narrowing in ZnO.[34] Hence the concentration of oxygen vacancy does become a measure of photocatlytic activity. A deconvolution of our PL spectra of the above three nanomaterials, reveals the presence of V^{+}_{O} emission at 2.22 eV. Oxygen vacancy concentration can be related to the area under the 2.24 eV emission curve which translates to the relative integrated intensity in the order: Mn/ZnO (15140) > ZnO (9179) > annealed Mn/ZnO (4916), the number in the parenthesis indicating the relative intensities in arbitrary units (See ESI Table S1 for the calculation). This order is in good agreement with photochemically generated H_2 from water (see Fig. 8). It is indeed a correlation between concentration of oxygen vacancy and quantity of $H_{2.}$ It may be noted that while the first material contains both oxygen vacancies and manganese ions, the second one contains only oxygen vacancies and the last one has only very few oxygen vacancies due to annealing with oxygen. It is inferred that addition of Mn^{2+} during the synthesis promotes the formation of more oxygen vacancies. The enhanced hydrogen production in Mn/ZnO can also be attributed to synergetic effect of manganese and V^{+}_{O} defect and latter may serve as active sites.[35] On the other hand in Mn/ZnO annealed under oxygen atmosphere the concentration of oxygen vacancies gets considerably reduced due to the incoming oxygen filling up the vacancies despite the presence of manganese. The latter metal plays a role in increasing such vacancies only during the synthesis, a significant point to be noted. The quantity of H_2 evolved of course is much smaller than those in ZnS/Mn or ZnS/Cu[36] systems but this is probably the first report on Mn/ZnO materials on water splitting experiment. We concede that the yield of H_2 is poor in this experiment and we feel that some more chemical modification and physical factors such as temperature change are necessary to improve its yield. Such kind of poor yield of H_2 in the catalytic reaction have been observed even in some preliminary works, up to ~100 µmol h^{-1} g^{-1} in perovskite lattices[33] and also in some ZnO materials.[34] He *et al.*[37] produces 29.8 µmol h^{-1} g^{-1} of hydrogen from Au/ZnO nanoparticles derived from zeolitic imidazolate framework-8 (ZIF-8) using 500 W light source. In a similar way, ZnO-ZnS hybrid nanowires shows 22 µmol h^{-1} g^{-1} of hydrogen using 300 W light source with UV- cut of filter.[38] While comparing the above results, the current work with the use of low power (150 W, metal halide) gives a much better yield. In addition, the microflowers of Mn/ZnO show good recyclability after 3 hr of light exposure as shown in ESI Fig. S4. Earlier, some chemical and physical modifications such as temperature, use of high power lamp have been found to generate a better yield of H_2 in strontium titanate nanomaterials.[33] However, precise understanding of the physical factors (reaction set up) is required to improve the productivity. Also a loss in H_2 evolution depending on reaction/reactor dynamics/conditions is possible during scaling up to gram level from our reported value of 60mg catalyst in our work

The quantum of oxygen vacancy, V^{+}_{O}, in these three materials decides their physical properties: EPR intensity of g~1.96 line, the intensity of deconvoluted PL emission from V^{+}_{O}, the intensity of the emission from F^{+} on exposure to X-ray as well as the quantity of H_2 production by visible light exposure with annealed Mn/ZnO < ZnO < as prepared Mn/ZnO.

Conclusions

In conclusion, the intrinsic defects of V^{+}_{O} with induced lattice parameter variations and high energy F^{+} centres have created a new route to achieve novel functionalities in technological applications. The oxygen vacancy emission of F^{+} centres enhances the visible light water splitting hydrogen production. However, additional experiments are required to improve the hydrogen productivity. It must also be noted that the intensity of light from F^{+} centres in Mn/ZnO is considerably reduced after annealing under oxygen, an additional effect of the concentration of oxygen vacancies. The same is true of EPR line at g~1.96 the intensity of PL emission due to V^{+}_{O}. The influences of V^{+}_{O} defects on magnetism and photocurrent properties and chemical modifications will be reported later.

Acknowledgements

PTM acknowledges the DST, Government of India for a research scheme (SR/S1/IC/0053/2012) and the INSA for a Senior Scientistship. BS is supported by an IIT/Madras Postdoctoral Fellowship and RJVM is supported partly by the above DST project of PTM.

Notes and references

1 A. B. Djurišić, W. C. H. Choy, V. A. L. Roy, Y. H. Leung, C. Y. Kwong, K. W. Cheah, T. K. Gundu Rao, W. K. Chan, H. Fei Lui and C. Surya, *Adv. Funct. Mater.*, 2004, **14**, 856–864.
2 A. B. Djurišić, Y. H. Leung, W. C. Choy, K. W. Cheah and W. K. Chan, *Appl. Phys. Lett.*, 2004, **84**, 2635–2637.
3 H.-L. Guo, Q. Zhu, X.-L. Wu, Y.-F. Jiang, X. Xie and A.-W. Xu, *Nanoscale*, 2015, **7**, 7216–7223.
4 K. Fink, *Phys. Chem. Chem. Phys.*, 2005, **7**, 2999–3004.
5 J. Becker, K. R. Raghupathi, J. St. Pierre, D. Zhao and R. T. Koodali, *J Phys. Chem. C*, 2011, **115**, 13844–13850.

6 D. Liu, Y. Lv, M. Zhang, Y. Liu, Y. Zhu, R. Zong and Y. Zhu, *J Mater. Chem. A*, 2014, **2**, 15377–15388.

7 S. G. Kumar and K. S. R. K. Rao, *RSC Advances*, 2015, **5**, 3306–3351.

8 A. McLaren, T. Valdes-Solis, G. Li and S. C. Tsang, *J. Am. Chem. Soc.*, 2009, **131**, 12540–12541.

9 A. K. -Radzimska and T. Jesionowski, *Materials,* 2014, *7*, 2833–2881.

10 R. J. V. Michael, B. Sambandam, T. Muthukumar, M. J. Umapathy and P. T. Manoharan, *Phys. Chem. Chem. Phys.,* 2014, **16**, 8541–8555.

11 T. I. Chanu, T. Muthukumar and P. T. Manoharan, *Phys. Chem. Chem. Phys.,* 2014, *16*, 23686–23698.

12 X. Lu, G. Wang, S. Xie, J. Shi, W. Li, Y. Tong and Y. Li, *Chem. Commun.,* 2012, **48**, 7717–7719.

13 S. Martha, K. H. Reddy and K. M. Parida, *J. Mater. Chem. A,* 2014, **2**, 3621–3631.

14 J. Huo, L. Fang, Y. Lei, G. Zeng and H. Zeng, *J. Mater. Chem. A,* 2014, **2**, 11040–11044.

15 P. Gao, Z. Liu and D. D. Sun, *J. Mater. Chem. A,* 2013, **1**, 14262–14269.

16 P. Gomathisankar, K. Hachisuka, H. Katsumata, T. Suzuki, K. Funasaka and S. Kaneco, *RSC Adv.,* 2013, **3**, 20429–20436.

17 B. Santara, P. Giri, K. Imakita and M. Fujii, *J. Phys. D: Appl. Phys.*, 2014, **47**, 215302.

18 L. Lamaita, M. A. Peluso, J. E. Sambeth, H. Thomas, G. Mineli and P. Porta, *Catal. Today*, 2005, **107–108**, 133–138.

19 P. Zhang, X. Li, Q. Zhao and S. Liu, *Nanoscale Res Lett.* 2011, **6**, 323.

20 M. Willander, O. Nur, J. R. Sadaf, M. I. Qadir, S. Zaman, A. Zainelabdin, N. Bano and I. Hussain, *Materials*, 2010, **3**, 2643–2667.

21 P. Zhan, W. Wang, C. Liu, Y. Hu, Z. Li, Z. Zhang, P. Zhang, B. Wang and X. Cao, *J. Appl. Phys.*, 2012, **111**, 033501.

22 B. Lin, Z. Fu and Y. Jia, *Appl. Phys. Lett.*, 2001, **79**, 943-945.

23 J.-w. Cai, J.-p. Xu, X.-s. Zhang, X.-p. Niu, T.-y. Xing, T. Ji and L. Li, *Optoelectron. Lett.*, 2012, **8**, 4–8.

24 D. C. Iza, D. Muñoz-Rojas, Q. Jia, B. Swartzentruber and J. L. MacManus-Driscoll, *Nanoscale Res. Lett.*, 2012, **7**, 655.

25 N. Alvi, K. Ul Hasan, O. Nur and M. Willander, *Nanoscale Res. Lett.*, 2011, **6**, 1–7.

26 B. Sotillo, Y. Ortega, P. Fernández and J. Piqueras, *CrystEngComm,* 2013, **15**, 7080–7088.

27 J. Jaćimović, Z. Micković, R. Gaál, R. Smajda, C. Vâju, A. Sienkiewicz, L. Forró, and A. Magrez, *Solid State Commun.,* 2011, **151**, 487–490.

28 H. Wang, S. Baek, J. Song, J. Lee and S. Lim, *Nanotechnology*, 2008, **19**, 075607.

29 M. Kowalik, R. Zalecki and A. Kolodziejczyk, *Acta Phys. Pol. A*, 2010, **117**, 277.

30 A. Janotti and C. G. Van de Walle, *Phys. Rev. B*, 2007, **76**, 165202.

31 C. Drouilly, J.-M. Krafft, F. Averseng, S. Casale, D. Bazer-Bachi, C. Chizallet, V. Lecocq, H. Vezin, H. Lauron-Pernot and G. Costentin, *J. Phys. Chem. C*, 2012, **116**, 21297–21307.

32 Y. Peng, Y. Wang, Q.-G. Chen, Q. Zhu and A. W. Xu, *CrystEngComm.*, 2014, **16**, 7906–7913.

33 H. Tan, Z. Zhao, W.-b. Zhu, E. N. Coker, B. Li, M. Zheng, W. Yu, H. Fan and Z. Sun, *ACS Appl. Mater. Interfaces*, 2014, **6**, 19184–19190.

34 J. Wang, Z. Wang, B. Huang, Y. Ma, Y. Liu, X. Qin, X. Zhang and Y. Dai, *ACS Appl. Mater. Interfaces*, 2012, **4**, 4024–4030.

35 X. Zhang, J. Qin, Y. Xue, P. Yu, B. Zhang, L. Wang and R. Liu, *Sci. Rep.*, 2014, **4**, 4596.

36 R. J. V. Michael, J. Theerthagiri, J. Madhavan, M. J. Umapathy and P. T. Manoharan, *RSC Adv.*, 2015, **5**, 30175–30186.

37 L. He, L. Li, T. Wang, H. Gao, G. Li, X. Wu, Z. Su and C. Wang, *Dalton Trans.,* 2014, **43**, 16981–16985.

38 Z. Wang, S. –W. Cao, S. C. J. Loo and C. Xue, *CrystEngComm,* 2013, **15**, 5688–5693.